HHS Public Access
Author manuscript
J Magn Reson Imaging. Author manuscript; available in PMC 2020 January 28.

Published in final edited form as:
J Magn Reson Imaging. 2018 December ; 48(6): 1468–1478. doi:10.1002/jmri.26271.

Emerging Role of MRI in Radiation Therapy

Hersh Chandarana, MD[1,2,*], **Hesheng Wang, PhD**[3], **R.H.N. Tijssen, DPhil**[4], **Indra J. Das, PhD**[3]

[1]Center for Advanced Imaging Innovation and Research (CAI2R), Department of Radiology, New York University School of Medicine, New York, New York, USA; [2]Bernard and Irene Schwartz Center for Biomedical Imaging, Department of Radiology, New York University School of Medicine, New York, New York, USA; [3]Department of Radiation Oncology, New York University School of Medicine & Laura and Isaac Perlmutter Cancer Center, New York, New York, USA; [4]Department of Radiotherapy, University Medical Center Utrecht, the Netherlands

Abstract

Advances in multimodality imaging, providing accurate information of the irradiated target volume and the adjacent critical structures or organs at risk (OAR), has made significant improvements in delivery of the external beam radiation dose. Radiation therapy conventionally has used computed tomography (CT) imaging for treatment planning and dose delivery. However, magnetic resonance imaging (MRI) provides unique advantages: added contrast information that can improve segmentation of the areas of interest, motion information that can help to better target and deliver radiation therapy, and posttreatment outcome analysis to better understand the biologic effect of radiation. To take advantage of these and other potential advantages of MRI in radiation therapy, radiologists and MRI physicists will need to understand the current radiation therapy workflow and speak the same language as our radiation therapy colleagues. This review article highlights the emerging role of MRI in radiation dose planning and delivery, but more so for MR-only treatment planning and delivery. Some of the areas of interest and challenges in implementing MRI in radiation therapy workflow are also briefly discussed.

Introduction to Radiotherapy for Cancer Treatment

The cancer mortality rate has decreased over the last century in men and women for almost all disease sites except glioblastoma and pancreatic cancer.[1] This is in part related to the advances in treatment resulting in better outcome and survival. In this context, radiation therapy (RT) is playing an increasing role as an important modality along with chemotherapy for the management of cancer patients in most disease sites.[2–4] It is estimate that 60% of cancer patients are treated with radiation in the management of their disease during their life span.[5] Even though cost effectiveness of radiation therapy is debated due to heavy initial cost of modern machines and use of national resources,[6] a true analysis

*Address reprint requests to: H.C., Department of Radiology, 660 1st Ave., 3rd Fl., New York, NY 10016. Hersh.Chandarana@nyumc.org.

provides a different picture, where radiation is cost-effective in the management of cancer patients.[7]

Advances in imaging, providing accurate information of the target volume (that is, the volume to be irradiated), and the adjacent critical structures or organs at risk (OAR), has made significant improvements in delivery of the external beam radiation dose. Radiation oncology has transitioned from a 2D approach to 3D conformal therapy (3DCRT) in 1990s. Additionally, modern advances with intensity-modulated radiation therapy (IMRT) and volumetric-modulated radiation therapy (VMAT) combined with inverse optimization in treatment planning has demonstrated a reduction in toxicity, as noted in a number of disease sites.[8–12] These techniques rely on imaging to appropriately plan and deliver radiation dose. Furthermore, more focused and hypofractionated beams for small targets such as stereotactic radiosurgery (SRS) and stereotactic body radiation (SBRT) has improved patient care by pinpointing the radiation delivery to the area of interest. Dose calculation from simple to more complex including inhomogeneity corrections have further tailored dose to the required sites. There are many aspects of progress in RT that are closely intertwined with imaging. These advances have improved planning and delivery of RT, resulting in superior outcome and reduction in toxicity with better quality of life for the cancer patients.

Current Workflow for RT Planning and Delivery

External beam radiation treatment involves a set of steps (Fig. 1) for precise and accurate dose delivery. The processes are immobilization, imaging for radiotherapy planning (computed tomography [CT], magnetic resonance imaging [MRI], positron emission tomography [PET]), image fusion, contouring (target volume and structure delineation), treatment planning including optimization, patient-specific quality assurance (PSQA), data transfer to the treatment device, pretreatment verification, and dose delivery. These steps could be modified or altered for some disease sites. A short description of the immobilization and imaging steps is described below.

Immobilization

As radiation treatment lasts several minutes, patient immobilization is critical for imaging and treatment. The success of radiation treatment is heavily dependent on the quality of immobilization. Immobilization devices play an important role in the disease-specific and site-specific RT such as prostate, lung, breast, and head and neck (Fig. 2). Immobilization devices are made out of materials with low electron density (such as plastic) that do not attenuate the beam, are nontoxic to the skin, and are comfortable for the patients for the duration of the treatment time, which can last up to 30 minutes. There is a wide array of immobilization devices for disease-specific sites and they are made either on-site or are standard devices that can be retrofitted or adjusted to the patient's body (such as a breast board). These devices are kept for the entire duration of the treatment, lasting a few days to as long as 45 days.

Imaging

Imaging is an essential component of the external beam RT planning for treatment delivery. Currently, most treatments use CT data for treatment planning, as it provides patient- and tissue-specific attenuation and electron density information. The emergence of CT-simulation[13] has changed the paradigm for treatment planning by providing patient-specific volumetric imaging data. It has replaced the regular radiographs with digital reconstruction radiographs (DRRs), which are created from the CT data.[14] Before advances in CT imaging, during treatment planning the radiation dose was computed with all tissues considered to have the same density (that of water). However, modern treatment planning and dose calculation relies on CT data that provides spatial 3D map of tissues attenuation values (Hounsfield Units, HU). The HU is converted into electron density, which is used to calculate tissue- and organ-specific doses.[15–19]

In current clinical practice, CT data are sometimes augmented with MRI and PET in the treatment of various malignancies. These images from other modalities are fused with CT data to take advantage of the superior soft-tissue contrast or metabolic information provided by these modalities. MRI provides unique and multiple contrast information. Furthermore, MRI contrast (such as T_1, T_2, and diffusion) could be tailored to highlight a specific organ or tumor. The sections below will briefly highlight the role of MRI in treatment planning and delivery. However, there are a number of challenges for MRI-only radiotherapy planning and delivery, including lack of electron density information and geometric distortion, which will also be addressed in this review.

MRI for Pretreatment Planning

The increased dosimetric conformity of modern treatment techniques, such as IMRT and VMAT, has generated new constraints on the accuracy of target delineation through imaging in RT. In order to deliver highly conformal treatments accurately, a precise definition of tumor and OAR is needed. This is the main reason MRI has seen increased usage in radiation oncology departments. Although in many cases CT still acts as the master reference scan, MRI provides superior soft-tissue contrast compared to CT, as well as a myriad of information on tumor characteristics that aid the delineation of both the tumor and OARs. The flexibility to acquire multiple contrasts has shown advantages for accurate tumor delineation in a large body of literature over the recent years. The American Association of Physicists in Medicine (AAPM) Task Group (TG-101)[20] on stereotactic body RT states that MRI is a gold-standard for visualization of brain tumors and "is increasingly used in SBRT applications including prostate, spinal tumors, chest, and solid abdominal tumors." MRI is routinely utilized in a number of malignancies (Table 1) for treatment planning (Figs. 3–4). T_2-weighted imaging, for example, is able to distinguish tumor from normal tissue and fat in rectal and esophageal cancer,[21] whereas T_1-weighted imaging provides good tumor contrast in squamous cell carcinoma in head and neck cancer.[22] Besides native T_1 and T_2 contrast, physiological contrasts such as dynamic contrast-enhanced (DCE), blood oxygen level-dependent (BOLD), and diffusion-weighted imaging (DWI) have been shown to have added value in defining tumor boundaries.[23–26] Physiological information from DCE, DWI, and BOLD imaging (often all referred to as functional imaging in the RT community) has been successfully used to derive tumor probability maps in prostate cancer, a major male cancer in the Western world.[27] This information was later used in a large Phase 3 trial, called the FLAME trial,[28] in which a focal micro boost up to 95 Gy in 35 fractions was given to the tumor (ie, GTV), while the prostate gland (ie, CTV) received a standard dose of 77 Gy in 35 fractions.

In a standard MRI-aided workflow, the acquired MRI data are registered to the planning CT on which the treatment plan is simulated. In order to minimize coregistration errors between the MRI and CT datasets, it is important that most imaging be performed in the treatment position (eg, flat tabletop with immobilization, as discussed in the section above). This, however, requires adaptations to the MRI workflow and the use of specialized imaging hardware. Most major MRI vendors themselves or in partnership with third-party suppliers offer special editions of their flagship 1.5T and 3T scanners that are equipped with tailored RT hardware and software. These options include more accurate laser positioning devices, flat tabletops that match the treatment table, coil bridges to prevent deformation of the patient's body contour, and fixation devices such as thermoplastic masks and arm supports, as shown in Fig. 2, but compatible in the magnetic field. The imaging protocols are also adapted to the specific requirements of treatment simulation. In comparison with diagnostic imaging, much more emphasis is put on the geometric accuracy of the imaging. The geometric accuracy of the preparatory scans determines the required safety margins,[29–32] and thus the amount of healthy tissue that is irradiated. Therefore, it is important to achieve the highest geometric accuracy possible. For this reason, RT scans are typically acquired at higher resolution and higher readout bandwidths, at the expense of signal-to-noise ratio (SNR). The push for 3D acquisitions is also higher than in diagnostic imaging, for two reasons: 1) the need to acquire isotropic resolution, and 2) the need to correct for gradient nonlinearity along all three dimensions. All these adaptations have to ensure that the MRI matches the planning CT as well as possible, because any misregistration would introduce a systematic error that propagates through the entire treatment.

A more recent trend is the use of MRI as the sole modality for RT: the so-called MRI-only workflow. A workflow in which all the preparatory steps are carried out on the MRI is favorable from a logistic point of view and removes the need to register the images to a separate planning CT, which potentially minimizes the risk of systematic error due to misregistration.[33–35] The major challenge for such a workflow is the assignment of electron densities to MRI scans for the dose calculation by the treatment planning system. However, partly due to the similar challenges that exist in PET/MR, a number of methods have been proposed in the literature that allows the generation of synthetic CT from MRI data. The methods range from voxel-based approaches that primarily use the information about voxel intensities, atlas-based approaches that register the images to a known (segmented) atlas, or hybrid approaches that use both. A brief discussion will follow but a comprehensive review has been published by Edmund and Nyholm.[36] More recently, deep learning approaches are gaining momentum and showing potential for success in converting MRI data to synthetic CT, especially where bone and air are present.[37–39]

Synthetic CT From MRI Data

Generation of Synthetic CT

The MR-only treatment planning can avoid potential error in MR-to-CT registration, and spare the cost and radiation from dedicated CT simulation. The emerging hybrid MR and linear accelerator technique[40] also motivates MR-only treatment planning to simplify the process of MR guidance in RT. However, unlike CT, there is no simple conversion from MR signal intensity to the electron density value that is required for accurate radiation dose calculation. Various methods have been proposed to generate pseudo-CT or CT-like images, also called synthetic CT (synCT) from MR images to replace CT data for radiotherapy treatment planning. These methods mostly utilize two types of information to establish a relationship between MR intensities and CT HUs: 1) tissue information derived from MR images, and 2) MR-to-CT correlation and transformation from a paired MR and CT dataset.

Tissue classification methods derive tissue content from MR images and apply the knowledge of bulk density of various tissue types to assign a CT number. The classification could be done by manual segmentation of T_1- or T_2-weighted MR images[41,42] or automatic intensity-based classification on multiple MR sequences.[43–45] Bone and air have low signals on conventional MR sequences. Thus, discriminating bone- and air-containing tissues remains a major challenge for intensity-based methods. The typical solution has been to include an ultrashort echo time (UTE) or zero-TE sequence data in the classification of bone and air.[44–47] However, it is important to note that including UTE and using multiple MR sequences increase scanning time, which may lead to motion artifacts and misalignment between images from different sequences. Other approaches that do not utilize additional imaging with UTE sequences include image segmentation methods such as a bone shape model[48] and active contour[49] to segment bone from T_1-weighted or DIXON MR images before classification of the remaining voxels for nonbone tissue. However, the accuracy of bone segmentation may still suffer from nearby air and artifact.

Although the appearances of MR and CT vary significantly, the spatial correlation between paired MR and CT could provide clues to constructing CT-like images from MRI data. Using MR images as signatures of associated CT, atlas-based methods generate synCT for patient MR by finding optimally matched atlas images.[50–52] These methods use conventional MR sequences but depend on the accuracy of deformable registration between atlas and patient MR. It is important to note that deformable registration is a challenging task, especially if the patient has pathological and/or anatomical differences from atlas images. To alleviate the inherent registration errors, the multi-atlas methods register patient MR to multiple atlases and fused associated CTs to generate synCT. Various multi-atlas methods have been proposed that use different approaches for fusing multiple atlas CTs, including voxelwise median,[53] probabilistic Bayesian analysis,[54] local image similarity,[55] and/or regional errors in the registration.[56] The multi-atlas registration and fusion was designed to increase robustness to registration errors, but nevertheless adds complexity and computation burden to the treatment planning workflow.

Instead of simply using spatial similarities in an MR-CT dataset, learning-based methods derive a map function to associate MR voxel intensities or image patches with HU numbers by supervised training on the atlas dataset. The mapping could be a regression function,[44,57,58] statistical decomposition,[59] random forest modeling,[60] or pattern recognition technique.[61] Recently, machine learning, especially deep learning and convolutional neural networks (CNNs),[62] has shown potential in this task of generating synthetic CT from MRI data. Han[37] built a U-Net-based CNN model[63] that consisted of an encoding part to learn from an input 2D MR slice and a decoding part to generate a corresponding 2D synCT slice. CNNs automatically learn multiple levels of information from a large set of MR-CT datasets. A CNN model[64] learned the mapping from a 3D multiple-parametric MR patches input to a same-size 3D synCT patch on a U-Net architecture. The model training takes a long time and a large amount of data, but synCT generation after training could be faster than classification or atlas-based approaches.

The aforementioned methods are more complementary than competitive. By using image classification for soft tissues and atlas registration for bone delineation, the hybrid method[64,65] generated synCT from DIXON MR without the need of a UTE sequence (Fig. 5). Gudur et al[54] combined T_1-weighted MR intensities and atlas-based geometry information to build a unified posterior probability density functions (PDF) for assigning the CT number. Continued advances will result in improved construction of synthetic CT from the MRI data.

Evaluation of Synthetic CT

SynCT have been developed and evaluated in support of MR-only treatment planning in a variety of anatomical sites,[66] including the brain,[67–69] head and neck,[45,70] and pelvis.[42,71,72] The majority of the studies were retrospectively performed on a small number of patients, usually in the range of 10–20. However, a recently performed prospective multi-center study of over 150 patients[73] validated MR-only prostate treatment planning using commercially available software. To replace CT in the treatment planning workflow, synCT is typically evaluated for the HU similarity between synCT and conventional planning CT and the equivalence of dose distributions calculated from the two datasets.

The mean absolute error (MAE) that is average of voxelwise absolute HU differences between synCT and CT is commonly used for synCT evaluation. The MAE should be calculated within the body contour but is often reported in different tissue regions, as there are great variations in HUs between different tissues. Instead of directly comparing voxelwise HU differences, geometric similarity between synCT and CT could be assessed by overlap of tissue volumes between the two images. The Dice similarity coefficient (DSC) for bone volumes has been reported for different methods and anatomical sites.[36] The external body contour is often generated automatically in treatment planning software using a threshold technique. Its spatial accuracy can be very important in dose calculation, especially for superficial tumors.[74] The DSC metric has been reported for geometrical accuracy of body volume, but it may be insensitive to the differences in the contours.[55]

Many studies have demonstrated the dosimetric equivalence of plan doses calculated on synCT and CT. These studies either recalculated a clinical plan generated from CT on corresponding synCT, or created a plan on synCT and recalculated it on CT to simulate an MR-only workflow. The synCT and CT-calculated doses are then compared for 3D dose distributions and dose-volume metrics. Absolute dose difference maps describe dosimetry agreement in 3D space,[72] but relatively large deviations are present at the boundaries of the body and target volume due to possible synCT-to-CT misalignment at the high dose gradient area. Gamma analysis composites both dose difference in low-dose gradients and distance to agreement (DTA) in high-dose gradients,[75] and is nearly unanimously reported in the literature for dose agreement assessment. The gamma index could be calculated on 3D dose volumes or 2D dose planes that may yield more stringent results.[76] Overall, gamma analysis across different methods and anatomical sites showed a >95% passing rate with clinically used criteria of 2% and 2 mm (dose-difference/DTA).[36,42,65,67,68,72]

Clinical assessment of a plan for treatment is largely based on dose-volume metrics for target volume and related OARs. The metrics are calculated from cumulative dose volume histograms of structures based on the guidelines of Quantitative Analysis of Normal Tissue Effects in the Clinic (QUANTEC).[77] The differences in reported metrics mostly were less than 2% and statistically insignificant[36,42,65,67,68,72] (Table 2). Wang et al[72] further applied the graphic technique to assess the equivalence of dose-volume metrics between the two image modalities. The clinically acceptable agreements in the available literature suggest that possible residual distortions in MR, synCT-to-CT local misalignment and HU deviations are of minor importance for dosimetric accuracy, likely due to the fact that doses of high-energy photons are relatively insensitive to small local electron density variations.[78,79]

Geometric Distortion

The essence of imaging for radiotherapy treatment guidance is geometric fidelity, as geometric distortions could directly lead to a misplacement of the radiation dose, thereby decreasing the effectiveness of the treatment and potentially increasing toxicity for nearby OAR. In diagnostic imaging, geometric distortions are normally only considered for acquisitions with long imaging readouts like echo-planar imaging (EPI) and distortion along a single readout line is usually ignored. For real-time MRI-guided RT, however, precision of <2 mm is required, so imaging is performed at much higher readout bandwidths (and thus lower SNR) compared to diagnostic imaging.[26,80] To further minimize off-resonance, corrections along the readout direction has been explored for treatment preparation scanning,[81] and for online MRI guidance.[82] To date, however, these methods have not yet been clinically introduced. DWI is a powerful imaging tool in oncology, and is often used for delineation guidance and treatment response monitoring. Due to the sensitivity to off-resonance distortion, EPI-based DWI is severely limited in head and neck and thoracic regions, even after distortion correction. For this reason, turbospin echo (TSE)-based DWI has seen renewed interest. DWI with a modified fast spin-echo acquisition (DW-SPLICE)[83] has been shown to be a viable, distortion-free alternative for imaging of head and neck patients at 3T,[84] but comes at the price of reduced SNR and prolonged imaging time due to the TSE readout, which hampers the transitioning to 1.5T.

Apart from off-resonance-induced distortion, distortions caused by gradient nonlinearities are also an important consideration. For diagnostic imaging, the vendor-provided corrections, performed during image reconstruction, may be adequate. For therapy guidance, however, these residual distortions need to be carefully characterized[85] and ideally further mitigated. Particularly for single-slice acquisitions, for which the gradient nonlinearity is only corrected in-plane, is still an unsolved issue for real-time image guidance. This through-plane slice distortion (referred to as potato chipping) could lead to local displacements of up to a few centimeters at locations 20 cm away from the isocenter.[86] Further work is needed to improve the geometric accuracy of various MR acquisition schemes and is an active area of investigation.

MR Guidance During Treatment

Over the last two decades the quality of external beam radiotherapy has advanced tremendously due to advances in pre- and postimaging such as on-board imaging methods like cone beam computer tomography (CBCT)[87] and electronic portal imaging devices (EPID).[88,89] The major limitation of the x-ray-based position verification is the poor soft-tissue contrast of these imaging modalities. Apart from lung tumors, tumor visualization is barely possible on clinical CBCT images, as shown in Fig. 6. Patient positioning is therefore often based on the bony anatomy in the vicinity of the tumor. Since a fixed relationship with bony anatomy (which can be well visualized on CBCT) cannot be established with great confidence, these uncertainties with respect to tumor position are dealt with by margins: the tumor volume is expanded to a much larger planning target volume, to make sure the tumor is always in the prescribed radiation beam. To stress this limitation: for these tumors it is accepted clinical practice that radio opaque markers (ie, fiducials) are implanted surgically, prior to radiotherapy, in order to allow “tumor-based” image registration on the linear accelerators (Fig. 7). This surgical procedure, however, is a substantial burden and risk to the patient.

The ultimate integration of MRI in modern radiotherapy is the use of MRI during the treatment session. Several groups are working on integrating MRI into the linear accelerator, resulting in hybrid MR-LINAC devices (Table 3). On-board MRI will allow position verification to be performed directly on the tumor, instead of nearby bony structures or implanted fiducials. Moreover, real-time MRI allows continuous tracking of the tumor position (Fig. 7) during radiation delivery. Depending on the type of motion, the treatment can be delivered in a gated fashion (eg, treatment delivery only during a certain respiratory phase), or fully tracked (in which the treatment beam follows the entire respiratory pathway).

The MRI-only pathway for RT has been suggested and implemented by many groups.[26,39,90–95] Such approaches have patient comfort, time delay, and financial burden for the multiple imaging in mind. However, many technical hurdles remain unsolved, such as geometric distortion and creation of universal synthetic CT.[25,96–98] An MR-only workflow, with or without MR-LINAC, will require suitable MRI-compatible immobilization devices, MRI sequences for disease-specific imaging for target and OAR delineation, synthetic CT generation, treatment planning, and then finally treatment. With a dedicated and integrated system, repeated MRI can play an increasing role in evaluation of treatment response, as suggested by number of research groups,[99–102] and briefly discussed below.

MRI for Treatment Assessment

The treatment response is usually evaluated by measuring the change in size of the tumor either in one dimension (RECIST and RECIST 1.1) or in two dimensions (WHO criteria). It is well understood that a change in size is a late measure of treatment response, and hence there is tremendous interest in developing biomarkers of early treatment response, especially in this era of targeted chemotherapies, immunotherapies, and combination of chemotherapy and RT.

MRI provides a unique opportunity to explore different contrast mechanisms to assess early treatment response. DWI is a functional MRI technique that is sensitive to the random microscopic motion (also known as Brownian motion) of the protons associated with water molecules. Highly cellular and complex tumor tissue impede mobility of the water molecule, resulting in high signal on DWI and corresponding low apparent diffusion coefficient (ADC). In response to therapy, tumor tissues will have decreased overall cellularity with increased necrosis. This will result in less restricted water molecules, resulting in low signal on DWI and correspondingly high ADC.

A number of studies have shown that changes in diffusion signal and ADC are helpful in predicting pathologic response to various tumor types, including locally advanced rectal cancer as well as cervical cancers undergoing combined neoadjuvant chemotherapy and radiation therapy (CRT).[103,104] In a recent study, post-CRT skewness of the ADC histogram and percentage change in ADC were useful for predicting a favorable response to neoadjuvant CRT in cervical cancer.[103] Similarly, in a small study of pancreatic cancer, there was an increase in ADC values of the pancreatic tumor after neoadjuvant chemoradiation.[105] Furthermore, posttreatment ADC values were correlated with degree of pathologic response.

DCE perfusion-weighted imaging (PWI) has also been explored in evaluation of treatment response after RT. However, this requires injection of exogenous gadolinium contrast agent. Other MRI endogenous contrasts such as arterial spin labeling (ASL), spectroscopy, T_1 and T_2 relaxation rates are promising and need further evaluation.

Conclusion

MRI is increasingly utilized in radiotherapy treatment planning due to improved contrast resolution of MRI compared to conventional CT. Furthermore, MRI will play an important role in the delivery of radiotherapy and in the assessment of treatment response in the near future, especially with introduction of the MR-LINAC systems. It will require close collaboration between radiation oncologists, radiologists, MR physicists, and RT physicists to take advantage of the unique capabilities of theses combined systems. Radiology and the MR community will need to understand the basics of RT planning and delivery and how MRI currently plays a role in radiotherapy treatment. This will enable development of novel MRI methods to tackle the unsolved problems and unmet need.

References

1. ACS. American Cancer Society. Cancer Facts and Figures 2015; http://www.cancer.org/acs/groups/content/@editorial/documents/document/acspc-044552.pdf. 2015
2. Hamdy FC, Donovan JL, Lane JA, et al. 10-Year outcomes after monitoring, surgery, or radiotherapy for localized prostate cancer. N Engl J Med 2016;375:1415–1424. [PubMed: 27626136]
3. Fisher B, Anderson S, Bryant J, et al. Twenty-year follow-up of a randomized trial comparing total mastectomy, lumpectomy, and lumpectomy plus irradiation for the treatment of invasive breast cancer. N Engl J Med 2002;347:1233–1241. [PubMed: 12393820]
4. Veronesi U, Cascinelli N, Mariani L, et al. Twenty-year follow-up of a randomized study comparing breast-conserving surgery with radical mastectomy for early breast cancer. N Engl J Med 2002;347:1227–1232. [PubMed: 12393819]
5. Citrin DE. Recent developments in radiotherapy. N Engl J Med 2017; 377:2200–2201.
6. Alhassani A, Chandra A, Chernew ME. The sources of the SGR "hole." N Engl J Med 2012;366:289–291. [PubMed: 22187962]
7. Lane JA, Donovan JL, Davis M, et al. Active monitoring, radical prostatectomy, or radiotherapy for localised prostate cancer: study design and diagnostic and baseline results of the ProtecT randomised phase 3 trial. Lancet Oncol 2014;15:1109–1118. [PubMed: 25163905]
8. Sheets NC, Goldin GH, Meyer A-M, et al. Intensity-modulated radiation therapy, proton therapy, or conformal radiation therapy and morbidity and disease control in localized prostate cancer. JAMA 2012;307: 1611–1620. [PubMed: 22511689]
9. Clavel S, Nguyen DHA, Fortin B, et al. Simultaneous integrated boost using intensity-modulated radiotherapy compared with conventional radiotherapy in patients treated with concurrent carboplatin and 5-fluorouracil for locally advanced oropharyngeal carcinoma. Int J Radiat Oncol Biol Phys 2012;82:582–589. [PubMed: 21277695]
10. Lee AW, Ng WT, Chan LL, et al. Evolution of treatment for nasopharyngeal cancer — Success and setback in the intensity-modulated radiotherapy era. Radiother Oncol 2014;110:377–384. [PubMed: 24630534]
11. Shirvani SM, Juloori A, Allen PK, et al. Comparison of 2 common radiation therapy techniques for definitive treatment of small cell lung cancer. Int J Radiat Oncol Biol Phys 2013;87:139–147. [PubMed: 23920393]
12. Freedman GM, Li T, Nicolaou N, et al. Breast intensity-modulated radiation therapy reduces time spent with acute dermatitis for women of all breast sizes during radiation. Int J Radiat Oncol Biol Phys 2009;74: 689–694. [PubMed: 19362779]
13. Coia LR, Schultheiss TE, Hanks GE. A practical guide to CT simulation. Madison, WI: Advanced Medical Publishing; 1995.
14. Das IJ, McGee KP, Desobrey GE. The digitally reconstructed radiograph: In: Coia LR, Schultheiss TE, Hanks GE (eds). A practical guide to CT simulation. Madison, WI: Advanced Medical Publishing; 1995 39–50.
15. Ahnesjö A, Saxner MA. A pencil beam model for photon beam calculation. Med Phys 1992;19:263–273. [PubMed: 1584117]
16. Ahnesjö A Collapsed cone convolution of radiant energy for photon dose calculation in heterogeneous media. Med Phys 1989;16:577–592. [PubMed: 2770632]
17. Fogliata A, Nicolini G, Vanetti E, et al. Dosimetric validation of the anisotropic analytical algorithm for photon dose calculation: fundamental characterization in water. Phys Med Biol 2006;51:1421–1438. [PubMed: 16510953]
18. Ojala J, Kapanen M, Sipila P, et al. The accuracy of Acuros XB algorithm for radiation beams traversing a metallic hip implant — Comparison with measurements and Monte Carlo calculations. J Appl Clin Med Phys 2014;15:162–176.
19. Ojala JJ, Kapanen MK, Hyodynmaa SJ, et al. Performance of dose calculation algorithms from three generations in lung SBRT: Comparison with full Monte Carlo-based dose distributions. J Appl Clin Med Phys 2014;15:4662. [PubMed: 24710454]

20. Benedict SH, Yenice KM, Followill D, et al. Stereotactic body radiation therapy: the report of AAPM Task Group 101. Med Phys 2010;37: 4078–4101. [PubMed: 20879569]
21. Beets-Tan RG, Beets GL. Local staging of rectal cancer: a review of imaging. J Magn Reson Imaging 2011;33:1012–1019. [PubMed: 21509856]
22. Becker M, Zbaren P, Casselman JW, et al. Neoplastic invasion of laryngeal cartilage: reassessment of criteria for diagnosis at MR imaging. Radiology 2008;249:551–559. [PubMed: 18936314]
23. Metcalfe P, Liney GP, Holloway L, et al. The potential for an enhanced role for MRI in radiation-therapy treatment planning. Technol Cancer Res Treat 2013;12:429–446. [PubMed: 23617289]
24. van der Heide UA, Houweling AC, Groenendaal G, et al. Functional MRI for radiotherapy dose painting. Magn Reson Imaging 2012;30: 1216–1223. [PubMed: 22770686]
25. Lagendijk JJ, Raaymakers BW, van Vulpen M. The magnetic resonance imaging-linac system. Semin Radiat Oncol 2014;24:207–209. [PubMed: 24931095]
26. Lagendijk JJ, Raaymakers BW, Van den Berg CA, et al. MR guidance in radiotherapy. Phys Med Biol 2014;59:R349–R369. [PubMed: 25322150]
27. Groenendaal G, Borren A, Moman MR, et al. Pathologic validation of a model based on diffusion-weighted imaging and dynamic contrast-enhanced magnetic resonance imaging for tumor delineation in the prostate peripheral zone. Int J Radiat Oncol Biol Phys 2012;82: e537–e544. [PubMed: 22197085]
28. Lips IM, van der Heide UA, Haustermans K, et al. Single blind randomized phase III trial to investigate the benefit of a focal lesion ablative microboost in prostate cancer (FLAME-trial): study protocol for a randomized controlled trial. Trials 2011;12:255. [PubMed: 22141598]
29. Moerland MA, Beersma R, Bhagwandien R, et al. Analysis and correction of geometric distortions in 1.5 T magnetic resonance images for use in radiotherapy treatment planning. Phys Med Biol 1995;40: 1651–1654. [PubMed: 8532746]
30. Paulson ES, Crijns SP, Keller BM, et al. Consensus opinion on MRI simulation for external beam radiation treatment planning. Radiother Oncol 2016;121:187–192. [PubMed: 27838146]
31. Stanescu T, Jaffray D. Investigation of the 4D composite MR image distortion field associated with tumor motion for MR-guided radiotherapy. Med Phys 2016;43:1550–1562. [PubMed: 26936738]
32. Stanescu T, Wachowicz K, Jaffray DA. Characterization of tissue magnetic susceptibility-induced distortions for MRIgRT. Med Phys 2012;39: 7185–7993. [PubMed: 23231269]
33. Roberson PL, McLaughlin PW, Narayana V, et al. Use and uncertainties of mutual information for computed tomography/magnetic resonance (CT/MR) registration post permanent implant of the prostate. Med Phys 2005;32:473–482. [PubMed: 15789594]
34. Ulin K, Urie MM, Cherlow JM. Results of a multi-institutional benchmark test for cranial CT/MR image registration. Int J Radiat Oncol Biol Phys 2010;77:1584–1589. [PubMed: 20381270]
35. Nyholm T, Nyberg M, Karlsson MG, et al. Systematisation of spatial uncertainties for comparison between a MR and a CT-based radiotherapy workflow for prostate treatments. Radiat Oncol 2009;4:54. [PubMed: 19919713]
36. Edmund JM, Nyholm T. A review of substitute CT generation for MRI-only radiation therapy. Radiat Oncol 2017;12:28. [PubMed: 28126030]
37. Han X MR-based synthetic CT generation using a deep convolutional neural network method. Med Phys 2017;44:1408–1419. [PubMed: 28192624]
38. Leynes AP, Yang J, Wiesinger F, et al. Direct PseudoCT generation for pelvis PET/MRI attenuation correction using deep convolutional neural networks with multi-parametric MRI: Zero echo-time and Dixon Deep pseudoCT (ZeDD-CT). J Nucl Med 2018;59:852–858. [PubMed: 29084824]
39. Largent A, Nunes JC, Lafond C, et al. [MRI-based radiotherapy planning.] Cancer Radiother 2017;21:788–798. [PubMed: 28690126]
40. Lagendijk JJ, Raaymakers BW, Raaijmakers AJ, et al. MRI/linac integration. Radiother Oncol 2008;86:25–29. [PubMed: 18023488]
41. Kim J, Glide-Hurst C, Doemer A, et al. Implementation of a novel algorithm for generating synthetic CT images from magnetic resonance imaging data sets for prostate cancer radiation therapy. Int J Radiat Oncol Biol Phys 2015;91:39–47. [PubMed: 25442341]

42. Kim J, Garbarino K, Schultz L, et al. Dosimetric evaluation of synthetic CT relative to bulk density assignment-based magnetic resonance-only approaches for prostate radiotherapy. Radiat Oncol 2015;10:239. [PubMed: 26597251]

43. Schulz V, Torres-Espallardo I, Renisch S, et al. Automatic, three-segment, MR-based attenuation correction for whole-body PET/MR data. Eur J Nucl Med Mol Imaging 2011;38:138–152. [PubMed: 20922522]

44. Johansson A, Karlsson M, Nyholm T. CT substitute derived from MRI sequences with ultrashort echo time. Med Phys 2011;38:2708–2714. [PubMed: 21776807]

45. Hsu SH, Cao Y, Huang K, et al. Investigation of a method for generating synthetic CT models from MRI scans of the head and neck for radiation therapy. Phys Med Biol 2013;58:8419–8435. [PubMed: 24217183]

46. Edmund JM, Kjer HM, Van Leemput K, et al. A voxel-based investigation for MRI-only radiotherapy of the brain using ultra short echo times. Phys Med Biol 2014;59:7501–7519. [PubMed: 25393873]

47. Keereman V, Fierens Y, Broux T, et al. MRI-based attenuation correction for PET/MRI using ultrashort echo time sequences. J Nucl Med 2010; 51:812–818. [PubMed: 20439508]

48. Liu L, Cao Y, Fessler JA, et al. A female pelvic bone shape model for air/bone separation in support of synthetic CT generation for radiation therapy. Phys Med Biol 2016;61:169–182. [PubMed: 26624989]

49. Bredfeldt JS, Liu L, Feng M, et al. Synthetic CT for MRI-based liver stereotactic body radiotherapy treatment planning. Phys Med Biol 2017; 62:2922–2934. [PubMed: 28306547]

50. Arabi H, Koutsouvelis N, Rouzaud M, et al. Atlas-guided generation of pseudo-CT images for MRI-only and hybrid PET-MRI-guided radiotherapy treatment planning. Phys Med Biol 2016;61:6531–6552. [PubMed: 27524504]

51. Uh J, Merchant TE, Li Y, et al. MRI-based treatment planning with pseudo CT generated through atlas registration. Med Phys 2014;41:051711. [PubMed: 24784377]

52. Dowling JA, Lambert J, Parker J, et al. An atlas-based electron density mapping method for magnetic resonance imaging (MRI)-alone treatment planning and adaptive MRI-based prostate radiation therapy. Int J Radiat Oncol Biol Phys 2012;83:e5–11. [PubMed: 22330995]

53. Sjolund J, Forsberg D, Andersson M, et al. Generating patient specific pseudo-CT of the head from MR using atlas-based regression. Phys Med Biol 2015;60:825–839. [PubMed: 25565133]

54. Gudur MS, Hara W, Le QT, et al. A unifying probabilistic Bayesian approach to derive electron density from MRI for radiation therapy treatment planning. Phys Med Biol 2014;59:6595–6606. [PubMed: 25321341]

55. Guerreiro F, Burgos N, Dunlop A, et al. Evaluation of a multi-atlas CT synthesis approach for MRI-only radiotherapy treatment planning. Phys Med 2017;35:7–17. [PubMed: 28242137]

56. Farjam R, Tyagi N, Veeraraghavan H, et al. Multiatlas approach with local registration goodness weighting for MRI-based electron density mapping of head and neck anatomy. Med Phys 2017;44:3706–3717. [PubMed: 28444772]

57. Korhonen J, Kapanen M, Keyrilainen J, et al. A dual model HU conversion from MRI intensity values within and outside of bone segment for MRI-based radiotherapy treatment planning of prostate cancer. Med Phys 2014;41:011704. [PubMed: 24387496]

58. Jonsson JH, Akhtari MM, Karlsson MG, et al. Accuracy of inverse treatment planning on substitute CT images derived from MR data for brain lesions. Radiat Oncol 2015;10:13. [PubMed: 25575414]

59. Siversson C, Nordstrom F, Nilsson T, et al. Technical Note: MRI only prostate radiotherapy planning using the statistical decomposition algorithm. Med Phys 2015;42:6090–6097. [PubMed: 26429284]

60. Huynh T, Gao Y, Kang J, et al. Estimating CT image from MRI data using structured random forest and auto-context model. IEEE Trans Med Imaging 2016;35:174–183. [PubMed: 26241970]

61. Hofmann M, Steinke F, Scheel V, et al. MRI-based attenuation correction for PET/MRI: a novel approach combining pattern recognition and atlas registration. J Nucl Med 2008;49:1875–1883. [PubMed: 18927326]

62. LeCun Y, Bengio Y, Hinton G. Deep learning. Nature 2015;521: 436–444. [PubMed: 26017442]

63. Ronneberger O, Fischer P, Brox T. U-Net: Convolutional Networks for Biomedical Image Segmentation, ArXiv e-prints, 2015.
64. Paulus DH, Quick HH, Geppert C, et al. Whole-Body PET/MR imaging: Quantitative evaluation of a novel model-based MR attenuation correction method including bone. J Nucl Med 2015;56:1061–1066. [PubMed: 26025957]
65. Wang H, Chandarana H, Block KT, et al. Dosimetric evaluation of synthetic CT for magnetic resonance-only based radiotherapy planning of lung cancer. Radiat Oncol 2017;12:108. [PubMed: 28651599]
66. Jonsson JH, Karlsson MG, Karlsson M, et al. Treatment planning using MRI data: an analysis of the dose calculation accuracy for different treatment regions. Radiat Oncol 2010;5:62. [PubMed: 20591179]
67. Paradis E, Cao Y, Lawrence TS, et al. Assessing the dosimetric accuracy of magnetic resonance-generated synthetic CT images for focal brain VMAT radiation therapy. Int J Radiat Oncol Biol Phys 2015;93: 1154–1161. [PubMed: 26581151]
68. Demol B, Boydev C, Korhonen J, et al. Dosimetric characterization of MRI-only treatment planning for brain tumors in atlas-based pseudo-CT images generated from standard T1-weighted MR images. Med Phys 2016;43:6557. [PubMed: 27908187]
69. Jonsson JH, Johansson A, Soderstrom K, et al. Treatment planning of intracranial targets on MRI derived substitute CT data. Radiother Oncol 2013;108:118–122. [PubMed: 23830190]
70. Chin AL, Lin A, Anamalayil S, et al. Feasibility and limitations of bulk density assignment in MRI for head and neck IMRT treatment planning. J Appl Clin Med Phys 2014;15:4851. [PubMed: 25207571]
71. Tyagi N, Fontenla S, Zhang J, et al. Dosimetric and workflow evaluation of first commercial synthetic CT software for clinical use in pelvis. Phys Med Biol 2017;62:2961–2975. [PubMed: 27983520]
72. Wang H, Du K, Qu J, et al. Dosimetric evaluation of magnetic resonance-generated synthetic CT for radiation treatment of rectal cancer. PLoS One 2018;13:e0190883. [PubMed: 29304105]
73. Persson E, Gustafsson C, Nordstrom F, et al. MR-OPERA: A multicenter/multivendor validation of magnetic resonance imaging-only prostate treatment planning using synthetic computed tomography images. Int J Radiat Oncol Biol Phys 2017;99:692–700. [PubMed: 28843375]
74. Korhonen J, Kapanen M, Keyrilainen J, et al. Influence of MRI-based bone outline definition errors on external radiotherapy dose calculation accuracy in heterogeneous pseudo-CT images of prostate cancer patients. Acta Oncol 2014;53:1100–1106. [PubMed: 24998163]
75. Low DA, Harms WB, Mutic S, et al. A technique for the quantitative evaluation of dose distributions. Med Phys 1998;25:656–661. [PubMed: 9608475]
76. Pulliam KB, Huang JY, Howell RM, et al. Comparison of 2D and 3D gamma analyses. Med Phys 2014;41:021710. [PubMed: 24506601]
77. Bentzen SM, Constine LS, Deasy JO, et al. Quantitative Analyses of Normal Tissue Effects in the Clinic (QUANTEC): an introduction to the scientific issues. Int J Radiat Oncol Biol Phys 2010;76:S3–9. [PubMed: 20171515]
78. Das IJ, Cheng CW, Cao M, et al. Computed tomography imaging parameters for inhomogeneity correction in radiation treatment planning. J Med Phys 2016;41:3–11. [PubMed: 27051164]
79. Cozzi L, Fogliata A, Buffa F, et al. Dosimetric impact of computed tomography calibration on a commercial treatment planning system for external radiation therapy. Radiother Oncol 1998;48:335–338. [PubMed: 9925254]
80. Paulson ES, Erickson B, Schultz C, et al. Comprehensive MRI simulation methodology using a dedicated MRI scanner in radiation oncology for external beam radiation treatment planning. Med Phys 2015;42:28–39. [PubMed: 25563245]
81. Walker A, Liney G, Holloway L, et al. Continuous table acquisition MRI for radiotherapy treatment planning: distortion assessment with a new extended 3D volumetric phantom. Med Phys 2015;42:1982–1991. [PubMed: 25832089]
82. Weygand J, Fuller CD, Ibbott GS, et al. Spatial precision in magnetic resonance imaging-guided radiation therapy: the role of geometric distortion. Int J Radiat Oncol Biol Phys 2016;95:1304–1316. [PubMed: 27354136]

83. Schick F SPLICE: sub-second diffusion-sensitive MR imaging using a modified fast spin-echo acquisition mode. Magn Reson Med 1997;38: 638–644. [PubMed: 9324331]
84. Schakel T, Hoogduin JM, Terhaard CHJ, et al. Technical note: Diffusion-weighted MRI with minimal distortion in head-and-neck radiotherapy using a turbo spin echo acquisition method. Med Phys 2017; 44:4188–4193. [PubMed: 28543364]
85. Tijssen RHN. Comprehensive MRI acceptance testing & commissioning of a 1.5 T MR-Linac: Guidelines and initial results, ESTRO 36 Vienna, Austria; 2017.
86. Borman PTS, Glitzner M, Tijssen RHN, et al. Estimation of non-correctible errors due to imperfections in imaging gradients. Presented at the 6th MRI in RT symposium, Utrecht, Netherlands; 2018.
87. Jaffray DA, Siewerdsen JH, Wong JW, et al. Flat-panel cone-beam computed tomography for image-guided radiation therapy. Int J Radiat Oncol Biol Phys 2002;53:1337–1349. [PubMed: 12128137]
88. Antonuk LE. Electronic portal imaging devices: a review and historical perspective of contemporary technologies and research. Phys Med Biol 2002;47:R31–65. [PubMed: 11936185]
89. Hsieh ES, Hansen KS, Kent MS, et al. Can a commercially available EPID dosimetry system detect small daily patient setup errors for cranial IMRT/SRS? Pract Radiat Oncol 2017;7:e283–e290. [PubMed: 28336480]
90. Johnstone E, Wyatt JJ, Henry AM, et al. Systematic Review of Synthetic Computed Tomography Generation Methodologies for Use in Magnetic Resonance Imaging-Only Radiation Therapy. Int J Radiat Oncol Biol Phys 2018;100:199–217. [PubMed: 29254773]
91. Walker A, Liney G, Metcalfe P, et al. MRI distortion: considerations for MRI based radiotherapy treatment planning. Australas Phys Eng Sci Med 2014;37:103–113. [PubMed: 24519001]
92. Liney GP, Moerland MA. Magnetic resonance imaging acquisition techniques for radiotherapy planning. Semin Radiat Oncol 2014;24: 160–168. [PubMed: 24931086]
93. Tenhunen M, Korhonen J, Kapanen M, et al. MRI-only based radiation therapy of prostate cancer: workflow and early clinical experience. Acta Oncol 2018;28:1–6.
94. Chen L, Price RA Jr, Wang L, et al. MRI-based treatment planning for radiotherapy: dosimetric verification for prostate IMRT. Int J Radiat Oncol Biol Phys 2004;60:636–647. [PubMed: 15380601]
95. Karlsson M, Karlsson MG, Nyholm T, et al. Dedicated magnetic resonance imaging in the radiotherapy clinic. Int J Radiat Oncol Biol Phys 2009;74:644–651. [PubMed: 19427564]
96. Mutic S, Dempsey JF. The ViewRay system: magnetic resonance-guided and controlled radiotherapy. Semin Radiat Oncol 2014;24:196–199. [PubMed: 24931092]
97. Keall PJ, Barton M, Crozier S. The Australian magnetic resonance imaging-linac program. Semin Radiat Oncol 2014;24:203–206. [PubMed: 24931094]
98. Fallone BG. The rotating biplanar linac-magnetic resonance imaging system. Semin Radiat Oncol 2014;24:200–202. [PubMed: 24931093]
99. Wu J, Tha KK, Xing L, et al. Radiomics and radiogenomics for precision radiotherapy. J Radiat Res 2018;59:i25–i31. [PubMed: 29385618]
100. Aerts HJ, Velazquez ER, Leijenaar RT, et al. Decoding tumour phenotype by noninvasive imaging using a quantitative radiomics approach. Nat Commun 2014;5:4006. [PubMed: 24892406]
101. Mattonen SA, Palma DA, Johnson C, et al. Detection of local cancer recurrence after stereotactic ablative radiation therapy for lung cancer: physician performance versus radiomic assessment. Int J Radiat Oncol Biol Phys 2016;94:1121–1128. [PubMed: 26907916]
102. Lambin P, Rios-Velazquez E, Leijenaar R, et al. Radiomics: extracting more information from medical images using advanced feature analysis. Eur J Cancer 2012;48:441–446. [PubMed: 22257792]
103. Bowen SR, Yuh WTC, Hippe DS, et al. Tumor radiomic heterogeneity: Multiparametric functional imaging to characterize variability and predict response following cervical cancer radiation therapy. J Magn Reson Imaging 2018;47:1388–1396. [PubMed: 29044908]
104. Enkhbaatar NE, Inoue S, Yamamuro H, et al. MR Imaging with Apparent Diffusion Coefficient Histogram Analysis: Evaluation of Locally Advanced Rectal Cancer after Chemotherapy and Radiation Therapy. Radiology 2018;288:129–137. [PubMed: 29558294]

105. Dalah E, Erickson B, Oshima K, et al. Correlation of ADC With Pathological Treatment Response for Radiation Therapy of Pancreatic Cancer. Transl Oncol 2018;11:391–398. [PubMed: 29455085]

Author Manuscript
Author Manuscript
Author Manuscript

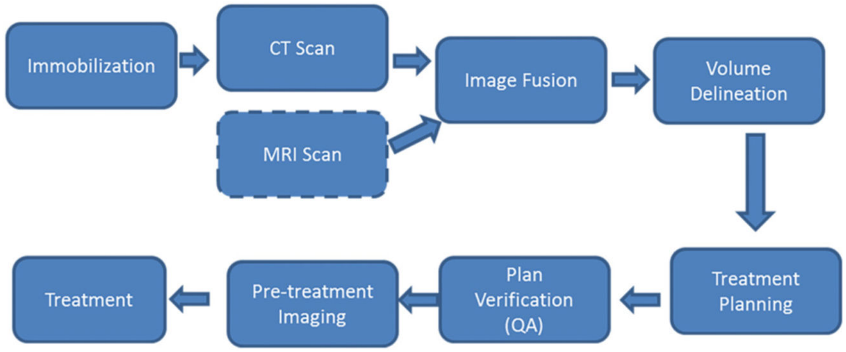

FIGURE 1:
Radiation treatment planning and delivery workflow.

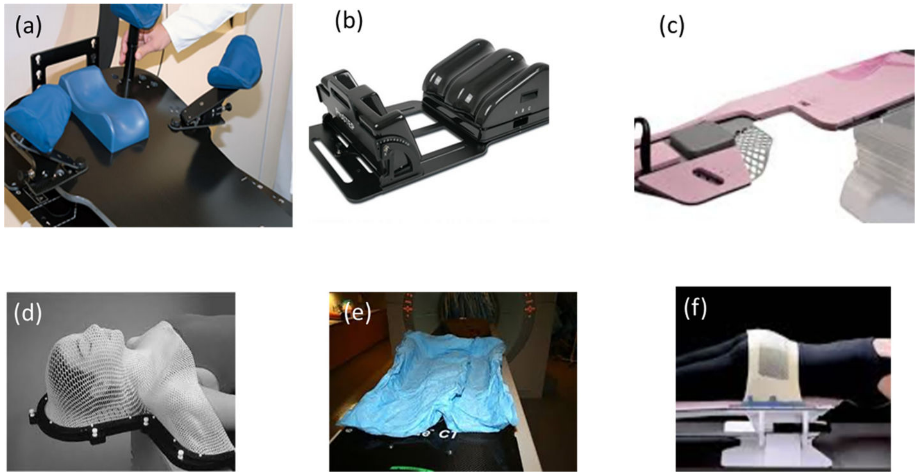

FIGURE 2:
Various types of immobilization devices. Upper panels are reusable and customizable to patient (a) breast and thorax board, (b) Leg support used in prostate, (c) prone breast board. Lower panels are patient specific fixation devices (d) aquaplast mold for head and neck, (e) Vaclock fixation used for trunk and (f) solid aquaplast device for pelvic immobilization.

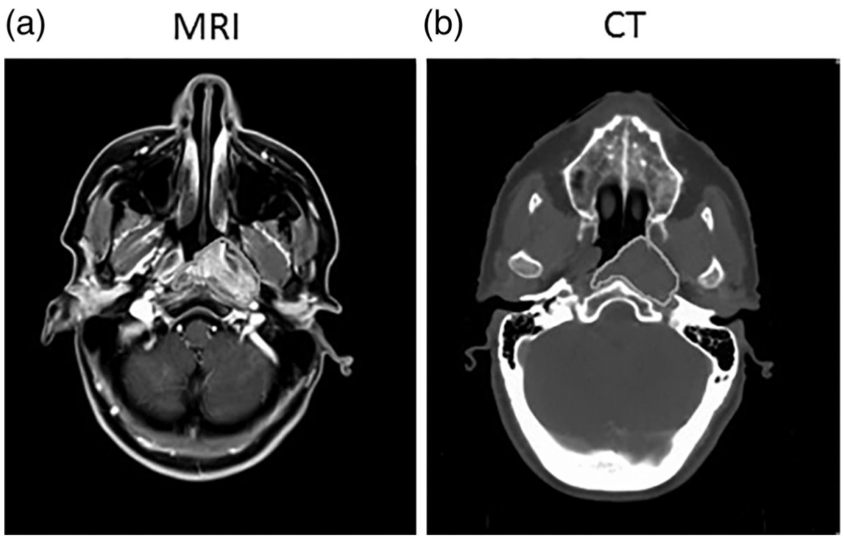

FIGURE 3:

Gross tumor volume (GTV) for head and neck cancer is delineated on pretreatment (a) MRI image which is registered to corresponding (b) CT dataset. MRI has higher contrast resolution, which enables tumor visualization and accurate GTV delineation, whereas CT images provide electron density information and are used for on-board registration with cone beam CT.

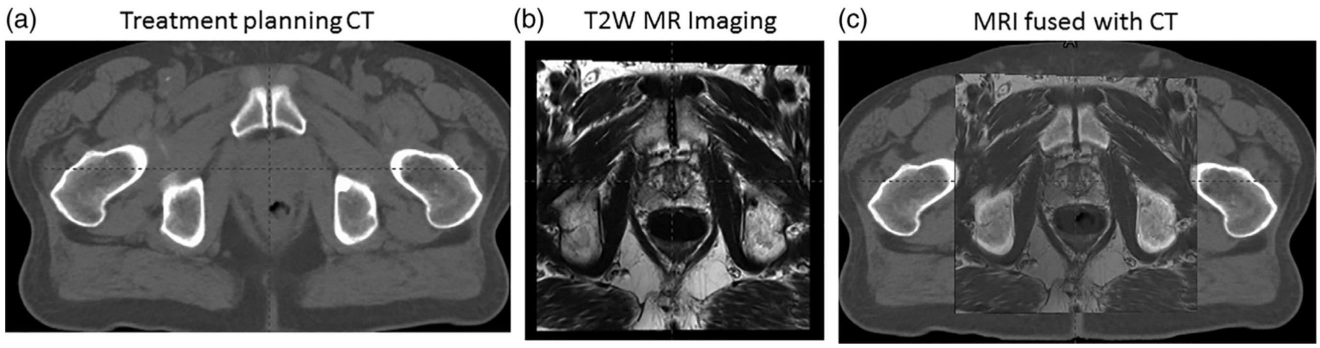

FIGURE 4:

(a) Treatment planning CT of the pelvis for prostate cancer. (b) T_2WI of the prostate. (c) Fused CT and MRI for external beam radiation therapy for prostate cancer.

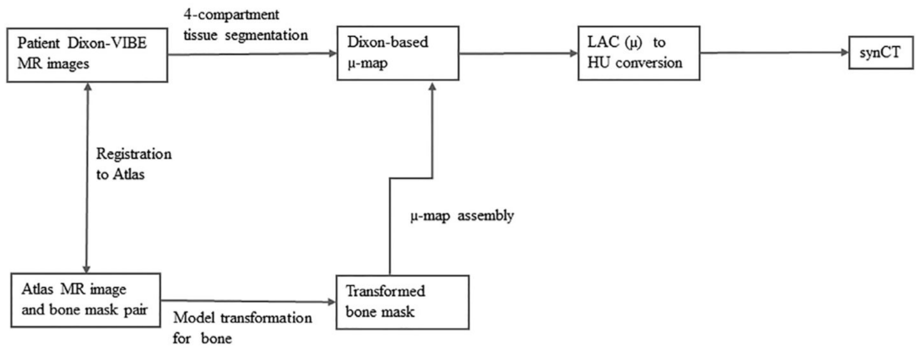

FIGURE 5:

Workflow of a hybrid method for synCT generation from Dixon MR images. These methods were initially proposed for PET/MR attenuation correction. μ is linear attenuation coefficient (LAC). SynCT is generated by converting the μ-map to HU numbers.

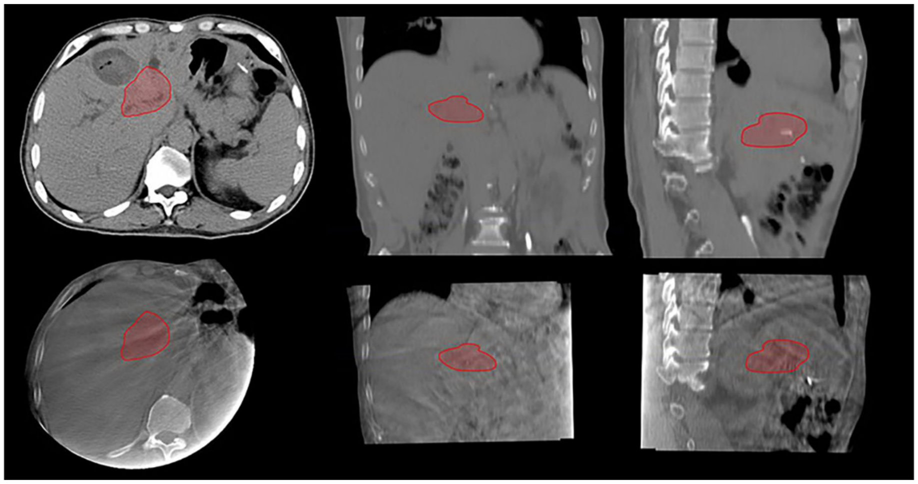

FIGURE 6:
Planning CT (top row) and cone beam CT (bottom row) of a liver tumor in axial, coronal, and sagittal views. Cone beam CT images are of inferior quality with poor visualization of the tumor. Red curve is the contour of the tumor obtained on the planning CT and copied to the Cone beam CT after image registration.

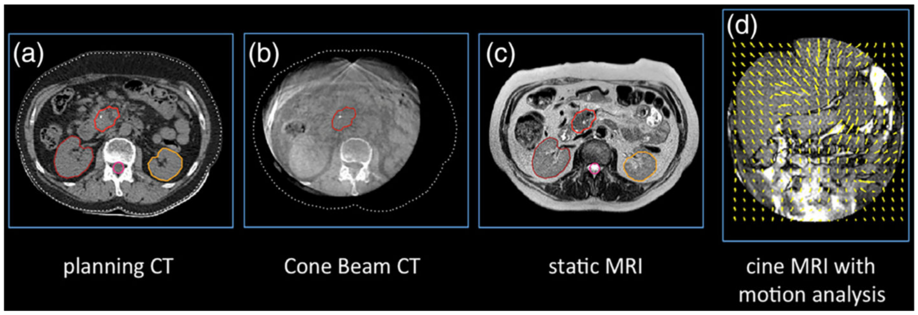

FIGURE 7:
Example images of a pancreatic tumor. The poor soft-tissue contrast in (a) CT and (b) Cone Beam CT necessitates the use of implanted fiducials in order to allow accurate tumor positioning on the LINAC. MRI on the other hand allows (c) direct visualization and (d) motion tracking of the tumor as well as organs at risk, which is essential for online treatment monitoring. No implanted fiducials are needed.

TABLE 1.

Examples of Common Malignancies for Which MRI is Routinely Utilized for Pretreatment Planning

Organ	
Brain	Better delineation of brain tumors on MRI as these tumors are not conspicuous on CT exam
Nasopharynx	Nasopharyngeal tumor are contoured on MRI and routinely fused with CT as shown in Fig. 3
Liver and pancreas	MRI is being increasingly utilized for hepatobiliary and pancreatic malignancy
Spine	Spinal tumor are visualized on MRI due to higher contrast resolution on Dixon and T2W images
Prostate	Prostate anatomy is not well visualized on CT and it can be difficult to delineate prostate from rectum. T2W MRI is helpful for visualization of prostate anatomy and tumor (Fig. 4)

TABLE 2.

Metrics Routinely Used for Evaluation of Dosimetric Agreement Between synCT and CT Calculated Plans

Tumor type	PTV dose metrics	OAR dose metrics
Brain tumor[67]	D95%, D5%, Dmax	Brainstem, optical nerves, eyes, lenses, chiasm, cochlea: Dmax
Head and neck cancer[55,56]	D98%, D2%, Dmean, Dmax	Parotid glands, submandibular glands, brain stem, spinal cord: D2%, Dmean, Dmax
Lung cancer[65]	D95%, D98%, D100%	Lung: V10Gy, V20Gy; Heart: V40Gy; Spinal cord: Dmax
Liver cancer[49]	D99%, D95%, D5%, D0.1cc	Colon, spinal cord, duodenum, esophagus, heart, stomach: D0.5cc
Prostate cancer[41,42]	D99%, D98%, D95%, D2%, Dmean, Dmax	Bladder, rectum: D35%, D25%, D15%, D2%, Dmean; Penile bulb: D90%
Pelvic cancer[48]	D99%, D0.5cc	Femur: V30Gy; Pelvis: V10Gy, V20Gy, Dmean; Rectum: V45Gy, Dmean; Sacrum: V10Gy, V20Gy; Bowel: D1cc, D5cc, V55Gy
Colorectal cancer[72]	D100%, D95%, D2%, Dmean	Bladder: V40Gy, Dmean; Bowel: V45Gy, Femoral head: V30Gy

PTV: planning target volume; OAR: organ at risk. A dose metric for a structure is calculated from dose volume histogram (DVH).

TABLE 3.

Overview of Some of the MR-LINAC Systems Either Currently Available Commercially or Being Actively Investigated in a Research Setting

ViewRay MRIdian, ** **Cleveland, USA**	**0.35 T MRI 3 Co sources / 6 MV Linac**
Elekta Unity, * Stockholm, Sweden	1.5 T MRI 7 MV Linac
Aurora-RT, MagnetTx, Edmonton, Canada	0.5 T MRI 6 MV Linac
Australian MRI-Linac, Ingham Institute, Liverpool, Australia	1.0 T MRI 4 & 6 MV Linac

* CE marked;

** CE marked and FDA cleared (June 2018).